ARTICLE

Molecular dynamics simulations on RORγt: insights into its functional agonism and inverse agonism

Cong-min Yuan[1], Hai-hong Chen[1], Nan-nan Sun[1], Xiao-jun Ma[1], Jun Xu[1] and Wei Fu[1]

The retinoic acid receptor-related orphan receptor (ROR) γt receptor is a member of nuclear receptors, which is indispensable for the expression of pro-inflammatory cytokine IL-17. RORγt has been established as a drug target to design and discover novel treatments for multiple inflammatory and immunological diseases. It is important to elucidate the molecular mechanisms of how RORγt is activated by an agonist, and how the transcription function of RORγt is interrupted by an inverse agonist. In this study we performed molecular dynamics simulations on four different RORγt systems, i.e., the apo protein, protein bound with agonist, protein bound with inverse agonist in the orthosteric-binding pocket, and protein bound with inverse agonist in the allosteric-binding pocket. We found that the orthosteric-binding pocket in the apo-form RORγt was mostly open, confirming that apo-form RORγt was constitutively active and could be readily activated (ca. tens of nanoseconds scale). The tracked data from MD simulations supported that RORγt could be activated by an agonist binding at the orthosteric-binding pocket, because the bound agonist helped to enhance the triplet His479–Tyr502–Phe506 interactions and stabilized H12 structure. The stabilized H12 helped RORγt to form the protein-binding site, and therefore made the receptor ready to recruit a coactivator molecule. We also showed that transcription function of RORγt could be interrupted by the binding of inverse agonist at the orthosteric-binding pocket or at the allosteric-binding site. After the inverse agonist was bound, H12 either structurally collapsed, or reorientated to a different position, at which the presumed protein-binding site was not able to be formed.

Keywords: RORγt; molecular dynamics simulation; agonism; inverse agonism; protein-binding site; orthosteric-binding pocket; allosteric-binding site

INTRODUCTION

Nuclear receptors (NRs) are ligand-regulated transcription factors [1]. The retinoic acid receptor-related orphan receptor (ROR) γt, as an NR, is only expressed in lymphoid organs, binds to the retinoid-related orphan receptor response element (RORE) within DNA to activate gene transcription, and has a constitutive level of activity even without binding to a ligand [2]. RORγt is indispensable for the pro-inflammatory cytokine interleukin IL-17 to be expressed from T-helper (Th)17 cells [3]. Th17 cells play a central role in the pathogenesis of autoimmune diseases such as rheumatoid arthritis, multiple sclerosis, psoriasis, and inflammatory bowel diseases, and are also actively involved in immunology processes [4–7]. As it is so important in multiple inflammatory and immunological pathways, RORγt has been established as a suitable drug target for the design and discovery of novel treatments for these diseases [1, 7–12].

Structurally, RORγt contains four different domains, namely, an N-terminal activation domain (activation function 1, AF1), a DNA-binding domain that binds the RORE in DNA via two zinc-finger motifs, a hinge region, and a C-terminal ligand-binding domain (LBD) [13–16]. The structure of the RORγt LBD features a three-layered fold of approximately 12 α-helices and 2–3 β-strands,

making a highly conserved hydrophobic orthosteric-binding pocket in its core structure and a protein-binding site near helix 12 (H12) for the binding of a cofactor [17–23]. The transcription function of RORγt can be easily modulated by a small ligand called a modulator. Once the RORγt LBD binds a modulator at its orthosteric-binding pocket, it is enabled to recruit either a coactivator or a corepressor to be bound at the protein-binding site. H12 (also called activation function 2, AF2) of the LBD is the essential structural component of the protein-binding site, and it can adopt distinct conformations in response to the binding of different modulators. Recent structural studies [17, 18, 20] revealed a new allosteric-binding site at the LBD that is formed by helices 4, 5, 11, and 12 and is far from the orthosteric-binding pocket (Fig. 1). After the binding of an agonist at the orthosteric-binding pocket, H12 at the LBD is stabilized in a conformation that is ready to interact with a coactivator, such as steroid receptor activator 2 (SRC2), at the protein-binding site. H12 can also be destabilized or completely reorientated after an inverse agonist is bound at the orthosteric-binding pocket or at the new allosteric site, thus repressing the gene transcription function of RORγt [15, 17, 19, 21]. Although this structural information has provided profound insights into how RORγt binds with an agonist or inverse

[1]Minhang Hospital and Department of Medicinal Chemistry at School of Pharmacy, Fudan University, 201203 Shanghai, China
Correspondence: Jun Xu (Aline_Adam@163.com) or Wei Fu (wfu@fudan.edu.cn)
These authors contributed equally: Cong-min Yuan, Hai-hong Chen, Nan-nan Sun

MD simulations on RORγt: insights into its agonism and inverse agonism
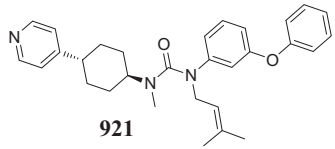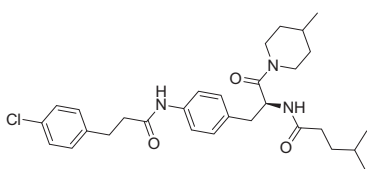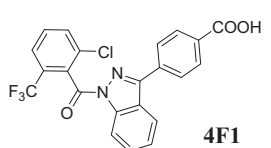CM Yuan et al.

1481

MATERIALS AND METHODS

MD simulations

The details of the MD simulations on the RORγt protein are listed in Table 1. Specifically, we started from crystal structures [17, 20] by selecting four PDB systems (the linker GGGG and the co-crystallized coactivator were removed) and named them PDB IDs. These systems include an apo-form of the RORγt protein (PDB entry 5VB3, resolution of 1.95 Å), the RORγt-agonist bound complex (PDB entry 5VB7, resolution of 2.34 Å), the RORγt bound with an orthosteric inverse agonist (PDB entry 5VB5, resolution of 2.23 Å), and the RORγt bound with an allosteric inverse agonist (PDB entry 5C4O, resolution of 2.24 Å). Each of the selected protein structures was visually checked and prepared by using the Protein Preparation Wizard encoded in the Schrodinger 3.5 software package [25]. Protonation states of ionizable residues and histidine residues were predicted according to the microenvironment and pKa values calculated with the PROPKA algorithm (http://propka.org) at pH = 7.0. Missing side chains and hydrogen atoms for each structure were complemented and minimized with restraints. To prepare the molecular topology files for each ligand, we directly extracted the ligand structure from the cocrystal structure and then generated the topological files using the PRODRG program [26]. Then, each system of protein structures was solvated in a cubic SPC water box with at least 10 Å from the box boundary to any residue. Na^+ and Cl^- ions were added to neutralize each solvated system and to maintain the ionic concentration at 0.15 M.

All MD simulation courses were carried out by using the Gromacs 5.1.4 package applied with the GROMOS96 43A1 force field [27]. Based on each of the prepared systems, energy minimization was performed first for the solvent molecules, including ions, and then on the protein and ligand molecule with constraints on protein backbone atoms [28]. After these two rounds of energy minimization, the whole system was minimized again without any constraints. During the energy minimization, we used the steepest descent algorithm and conjugate gradient algorithm successively [27]. Afterwards, each system was equilibrated at 50, 100, 200, and 310 K for 10 ps each, followed by NPT equilibration for 20 ps at 310 K. The Langevin Nosé–Hoover thermostat [29, 30] and the Parrinello–Rahman method [31, 32] were employed to maintain each system at a constant temperature and a constant pressure of 1 atm. All bonds were constrained by the LINCS algorithm [33]. The van der Waals interaction cutoff was set to 12 Å, while long-range electrostatic interactions were calculated using the particle mesh Ewald method [34, 35] with a grid size of 1.2 Å. The time step was set as 2 fs with coordinates saved every 10 ps for the purpose of analysis. The periodic boundary conditions were implemented in all directions along the simulation box. After equilibration of the system, the production MD simulations were run for 150 ns for each system.

Data analysis

We performed all the analyses based on the trajectories of the MD production stage. The conformations of each trajectory were clustered by the tools inside the Gromacs 5.1.4 package. The representative structure of each system was derived from the largest conformational cluster based on the MD trajectories [36]. The DSSP program [37] was applied to standardize the secondary structure assignment of two helices (H11′ and H12). To reveal the most important internal motion of each simulated system, we performed principal component analysis (PCA) [38–40] on the MD trajectories. Briefly, we used the starting system as the reference structure and performed a least square fitting of the MD trajectory to the reference structure [41, 42]. The covariance matrix was built and diagonalized, and the first principal component was plotted by the convenient tools implemented inside the Gromacs 5.1.4 package. All the structural graphics were processed with the PyMOL software [43].

Orthosteric binding site

Fig. 1 Orthosteric-binding site (yellow) and allosteric-binding site (green) of RORγt protein. X-ray structures superimposition of PDB 5VB5 (yellow) and 5C4O (green) based on their Cα atoms

agonist and where H12 of the LBD could interact with or reorient relative to the neighboring structural components, the mechanisms of these conformational changes resulting from ligand binding remain ambiguous. For example, how does the binding of an agonist at the orthosteric-binding pocket cause the stabilization of H12 and therefore help the RORγt in recruiting the coactivator? How does an inverse agonist binding at the orthosteric-binding pocket or at the allosteric-binding site perturb the protein-binding site? This event leads to H12 destabilization and the coactivator not being able to bind. It has been suggested that the binding of an agonist or inverse agonist can switch on or off the transcriptional activity of RORγt and that the dynamic conformational equilibrium is a fundamental attribute of this receptor. We think it is important to understand the molecular mechanisms underlying the conformational dynamics of RORγt and their relationship to its transcription function [24]. Such understanding of the dynamic conformational equilibrium is also important and helpful for the future design of novel RORγt modulators (agonists or inverse agonists) with better pharmacokinetic and/or pharmacodynamic properties, such as improved cellular activity, potent inhibition of IL-17 release, and better oral bioavailability.

In the present study, we selected a system of RORγt without ligand binding (apo-form) and three typical systems of RORγt bound with different modulators: agonist, inverse agonist bound at the orthosteric-binding pocket, and inverse agonist bound at the allosteric-binding site. We conducted molecular dynamics (MD) simulations on all four RORγt systems to track the intramolecular and intermolecular interactions. The results from our MD simulations confirm that the apo-form RORγt is constitutively active. We also demonstrated that the binding of agonist stabilizes H12 and that the binding of inverse agonist makes H12 completely collapse or reorient to a different position. Once H12 of RORγt is not able to partly form the presumed protein-binding site, the transcription function of the receptor is disrupted. These insights into the inherent conformational dynamics of RORγt will be very helpful for the design of ligands with greater potency and specificity (agonists and/or inverse agonists) that could be used as potential treatments for RORγt-related health problems.

MD simulations on RORγt: insights into its agonism and inverse agonism
CM Yuan et al.

1482

Table 1. Detailed information of MD simulations for the four RORγt systems

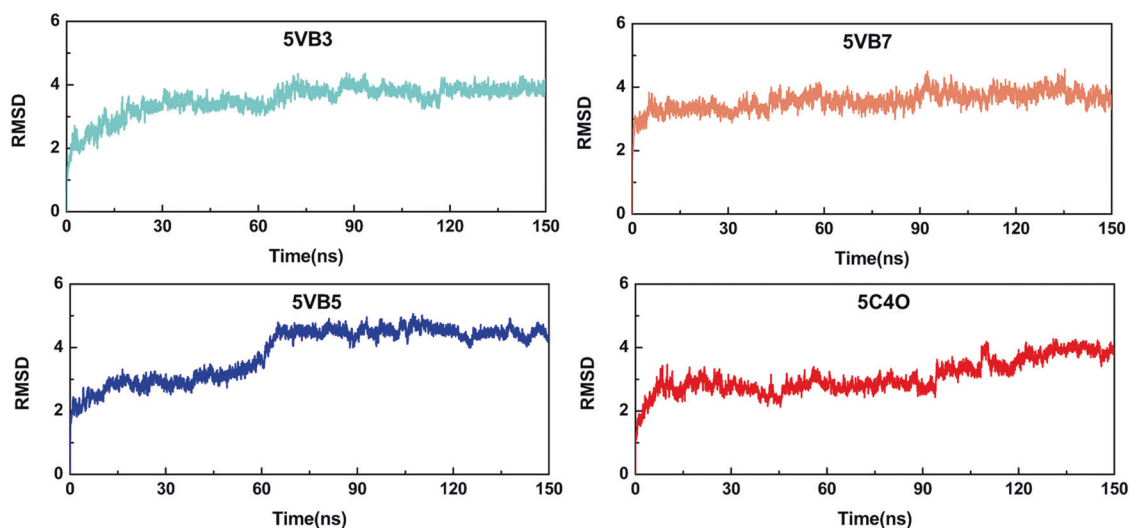| Systems	System size (Å)	Residues	Ligand*	Type	Binding site
5VB3	53*56*42	265-507	-	apo	-
5VB7	56*55*43	265-507	**921**	agonist	
5VB5	56*53*43	265-507	**92A**	inverse agonist	orthosteric
5C4O	43*63*46	267-507	**4F1**		allosteric

Fig. 2 Positional rmsd (in Å) for Cα atoms of each of the simulated systems along the simulation time (ns), and labeled with the PDB IDs

RESULTS AND DISCUSSION

Stability of the simulation systems

For the purpose of comparing the simulated structures, we superimposed the starting structure of each system onto the apo-form structure, 5VB3. As shown in Fig. S1 of the Supporting Information, the X-ray structures of the apo-form in 5VB3, agonist-bound form in 5VB7, and form bound with an inverse agonist at the orthosteric-binding pocket in 5VB5 could be superimposed very well (Fig. S1a) with small overall positional root-mean square deviation (rmsd) values (rmsd for Cα atoms of 5VB7 vs. those of 5VB3 was 0.367 Å, 5VB5 vs. 5VB3 as 0.178 Å). The Cα rmsd between the 5C4O protein structure bound with the inverse agonist at the allosteric-binding site and the 5VB3 structure is 0.66 Å (Fig. S1b), and an obvious difference exists at H11, H11', and H12 (Fig. S1c).

Figure 2 shows the time-dependent rmsd curve of Cα atoms for each simulated system based on the starting X-ray structure. As the simulations progressed, each of the systems fluctuated for a short period of time, ca. 5–10 ns, and then the rmsd curve became very flat until the end of simulation at 150 ns. However, in the 5VB5 system, the rmsd curve flattened at approximately 60 ns,
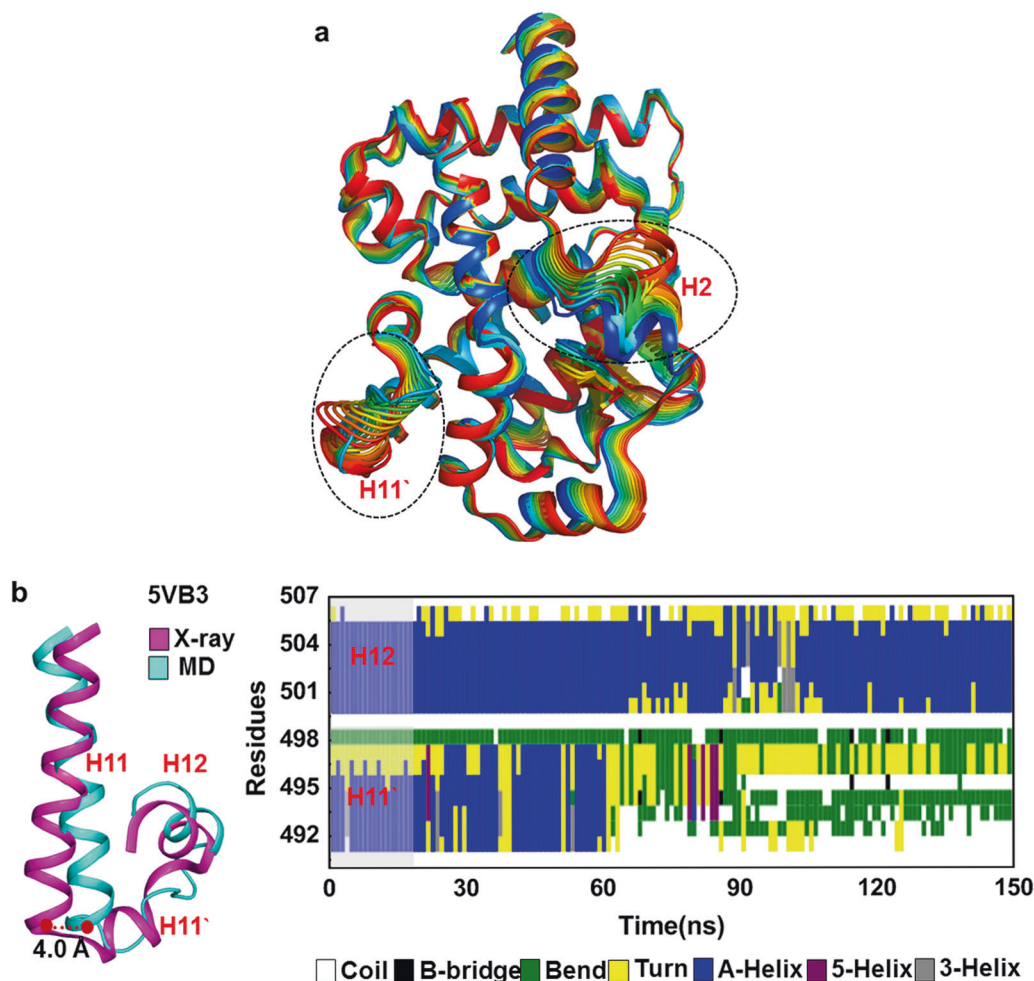
MD simulations on RORγt: insights into its agonism and inverse agonism
CM Yuan et al.

1483

Fig. 3 Results of structural monitoring of the apo-form RORγt 5VB3 from the MD trajectory. **a** The plot of PCA analysis for the whole LBD structure, where the H2 and H11′ are labeled. **b** The tracked changes in the secondary structure of H11′ and H12, which were calculated by using the DSSP software [37]. Left panel: a typical conformation of H11–H11′–H12 (colored in cyan) derived from the largest conformational cluster of the MD trajectory, is superimposed onto the starting X-ray structure (colored in purple). Right panel: secondary structure changes of H11′ and H12 along the simulation time

which was attributed to collapsed H11′ and H12 (the details will be discussed later). In general, each of the simulations proceeded smoothly, and the protein structure was quite stabilized by the solvent molecules.

Conformational dynamics of the Apo-form of RORγt
In a recent report on the X-ray structure of RORγt [20], it was claimed that the apo-form, i.e., the ligand-free structure, was able to maintain an active state based on two observations. The first observation was that H12 was in an active conformation similar to the conformation of H12 in the coactivator-bound structure (PDB entry 3L0L). H12 was stabilized by intramolecular interactions of the triplet residues His479–Tyr502–Phe506. Another observation was from the solution NMR studies, which showed distinctive chemical shift perturbations at the backbone atoms with titration of coactivator SRC2. To confirm that the apo-form RORγt is active and ready to bind coactivator if provided, we performed PCA and DSSP [37] calculations to track the secondary structure of H11′ and H12 based on the MD trajectory. As shown in Fig. 3a, the plot of PCA results suggests that the apo-form RORγt does have some structural flexibility and that the helices H2 and H11′ are the most flexible parts of the structure. As helix H2 is located at the entrance of the orthosteric-binding pocket, its structural fluctuation indicates that the orthosteric-binding pocket is open and

ready to accept a ligand. The secondary structure contents of H11′ and H12 (Fig. 3b) indicate that H11′ uncoiled entirely, from helix to random coil, at approximately 60 ns into the MD trajectory. As a result of the structural change in H11′, the helix H11 tilted toward the helix H12. During this process, H12 was maintained as a regular α-helix and packed well with H11 (Fig. 3b).

Tracking of the positions of the triplet residues His479–Tyr 502–Phe506 from the MD trajectory reveals the important details of their intramolecular interactions. As shown in Fig. 4, residue His479 from H11 formed a constant hydrogen bond with the hydroxyl group at the side chain of Tyr502 from H12 (Fig. 4b), being maintained for 85.2% of the MD trajectory (black curve of Fig. 4a). The side chain of His479 also formed a typical edge-to-face and/or face-to-face π–π interaction with the aromatic side chain of Phe506 (blue curve of Fig. 4a) for 85.9% of the the MD simulations (the cutoff distance from the center of the His479 side chain to the center of the Phe506 side chain was 6.5 Å). There was also an intermediate π–π stacking interaction between the aromatic side chain of Tyr502 and the side chain of Phe506 that was present 95.6% of the whole MD trajectory (red curve of Fig. 4a, and cutoff distance from the center of the Tyr502 side chain to the center of the Phe506 side chain was 6.5 Å). All of these data of tracked distances suggest that the triplet residues His479–Tyr502–Phe506 had strong intramolecular interactions.
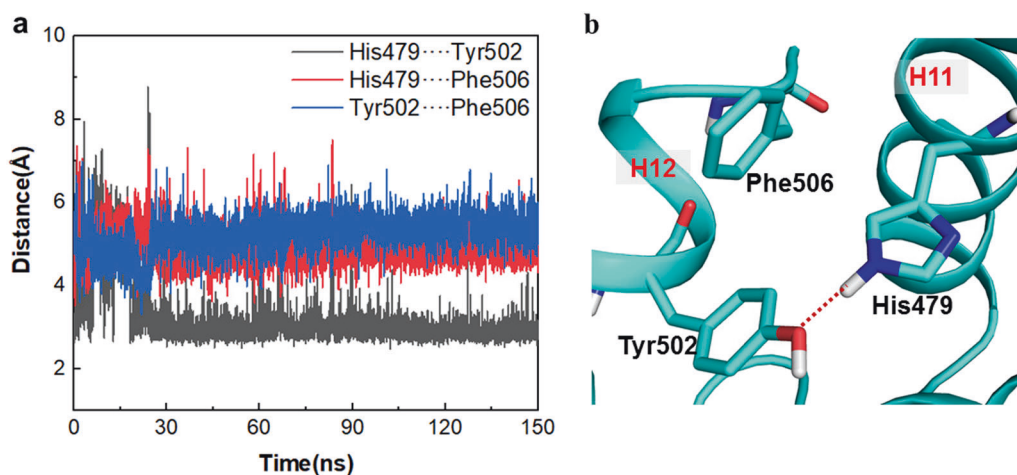
MD simulations on RORγt: insights into its agonism and inverse agonism
CM Yuan et al.

1484

Fig. 4   The dynamics of the triplet H479-Y502-F506 in 5VB3 system along the MD trajectory. **a** Tracked distances between each pair of these three residues. **b** The hydrogen-bonding interaction between the side chain of His479 from H11 and the side chain of Tyr502 from H12, which is represented as red dashed line, with the cutoff criterion that the distance from the nitrogen atom at His479 side chain to the oxygen atom at the Tyr502 side chain is less than 3.5 Å. These triplet residues are shown as sticks and the protein as ribbon in cyan color
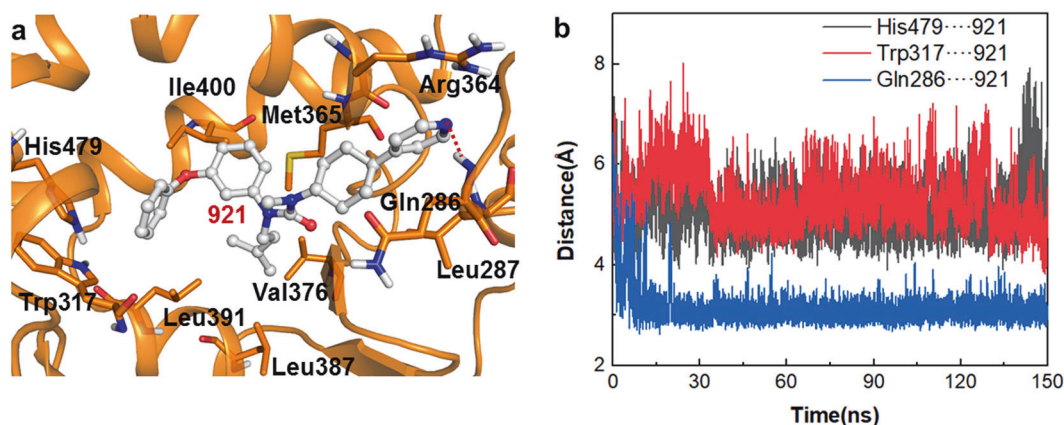

Fig. 5   RORγt 5VB7 binding with agonist compound **921**, and the intermolecular interactions. **a** The agonist **921** (shown in ball-and-stick style) at the orthosteric-binding pocket displayed with important residues. Hydrogen bonds are represented as red dashed lines. **b** The tracked distances between the important residues and the agonist **921**. The His479—**921** stands for the distance from the center of His479 side chain to the center of the phenyl group at the tail of agonist **921**, the Trp317—**921** stands for the distance from the center of Trp317 side chain to the center of the phenyl group at the tail of **921**, and the Gln286—**921** for the distance from the backbone nitrogen atom of Gln286 to the nitrogen atom at the pyridine head group of agonist **921**

Such hydrogen-bonding and aromatic packing interactions are the most important structural determinants allow H12 to maintain a regular α-helix structure.

Mode of action for RORγt binding an agonist

As reported in previous structural studies [7, 13, 20–23], the sandwich-like RORγt LBD contains an orthosteric-binding pocket formed by helices H2, H3, H5, and H11 at its central layer. This pocket is mainly hydrophobic and large enough (~940 Å³) to accommodate ligands of various sizes and shapes [13, 20, 22]. As shown in Fig. 5a, for the binding structure derived from the trajectory of the MD product, agonist **921** sits very well inside this orthosteric-binding pocket, with its pyridine head group located near the entrance of the pocket and its phenyl tail reaching the bottom of the binding site (Fig. 5a). The isobutylene group of agonist **921** packs tightly with hydrophobic side chains of residues Val376, Leu387, Leu391, and Leu396. The tracked dynamics from MD simulations (Fig. 5b) show that most of these receptor-agonist interactions are persistent. For example, the pyridine head group formed a constant hydrogen-bonding interaction with the backbone amide hydrogen atom of Gln286 for 93.5% of the simulation, and the phenyl ether group of agonist **921** formed π–π interactions with the aromatic side chain of Trp317 96.7% of the time and with the His479 side chain 98.7% of the simulation time. The π–π interactions of the phenyl head of **921** with His479 and Trp317 form a hydrophobic cluster. His479 is in the middle of the cluster and forms a face-to-face π–π interaction with both the side chain of Trp317 and the phenyl head of **921**, indicating the important role of His479.

Since agonist **921** is bound tightly at the orthosteric-binding pocket, we wanted to know how the agonist binding affects H12 and the protein-binding site. For this purpose, we tracked the changes of the triplet His479–Tyr502–Phe506 through the MD trajectory. As shown in Fig. 6, these typical intramolecular interactions are conserved in the presence of agonist **921**. The His479–Tyr502 hydrogen-bonding interaction survived well, retained for 74.8% of the simulation (based on the same criterion as in Fig. 4). The π–π interactions between the side chains of the His479–Tyr502 pair remained for 98.2% of the simulation, and 100% for the Tyr502–Phe506 side chain interactions.

MD simulations on RORγt: insights into its agonism and inverse agonism
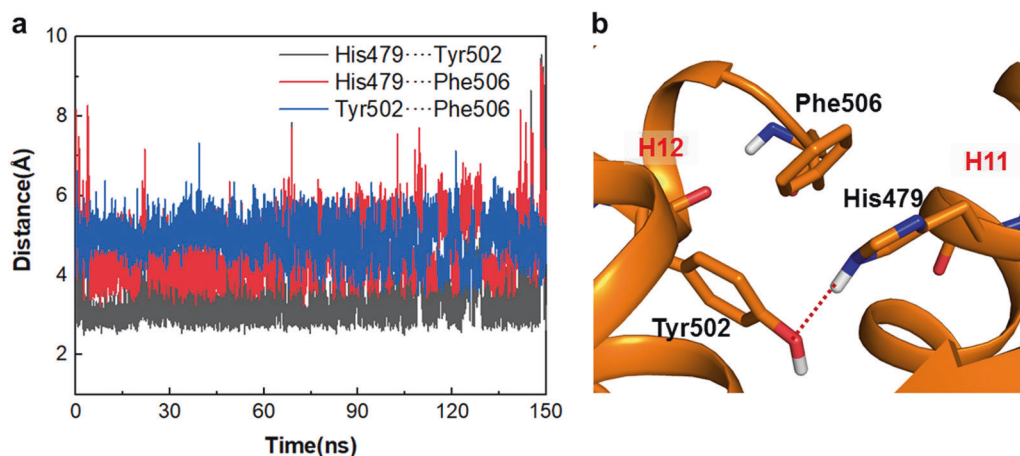CM Yuan et al.

1485

Fig. 6 **a** The tracked distances for the triplet H479–Y502–F506 of agonist-bound RORγt 5VB7 system through the MD trajectory. **b** The hydrogen-bonding interaction between the side chain of His479 from H11 and the side chain of Tyr502 from H12 is represented as red dashed line, and the cutoff is 3.5 Å for the distance from the nitrogen atom at His479 side chain to the oxygen atom at the Tyr502 side chain. These triplet residues are shown as sticks and the protein as gold ribbon

In addition to the persistence of the triplet interactions, we tracked the secondary structures of H11′ and H12, which are presented in Fig. 7a. H12 is able to orientate in a position very similar to that in the starting structure (left panel of Fig. 7a), and keeps its helical structure (right panel of Fig. 7a). The PCA plot (Fig. 7b) shows that the agonist-bound RORγt LBD is much less flexible than the apo-form RORγt (Fig. 4a). Although H11′ is flexible to some extent (Fig. 7b), it is mostly helical throughout the MD simulations (right panel of Fig. 7a). As shown in Fig. 7c, the hydrophobic cluster at the protein-binding site is also well maintained, with two hydrophobic residues (Leu501 and Leu505) from H12. This dynamic information of the RORγt 5VB7 system denotes the mode of action for agonism of RORγt. That is, after agonist **921** is bound inside the orthosteric-binding pocket, H12 is stabilized by the triplet His479–Tyr502–Phe506 interactions and maintains its structure as a typical helix. The stabilized H12 helps to form the protein-binding site so the receptor is ready to recruit a coactivator such as SRC2.

Inverse agonism for RORγt by the binding at the orthosteric pocket
RORγt is constitutively active [2]. The results of our MD simulations on the apo-form structure confirmed that the orthosteric-binding pocket is mostly open (Fig. 3a) and that the triplet His479–Tyr502–Phe506 residues interact with each other through hydrogen-bonding and aromatic π–π packing (Fig. 4). A straightforward way to interrupt the transcription function of RORγt is to design organic molecules that are able to more fully occupy the large orthosteric-binding pocket so that its unique triplet interactions are destabilized or lost. Following this strategy, many more efforts have been focused on the discovery of RORγt inverse agonists in recent years [8–10, 12, 14, 18–23]. Compound **92A** is a typical inverse agonist, and it sterically clashes with the side chain of His479 [20]. As shown in Fig. 8, regarding the dynamics of RORγt-**92A** binding, the side chain of His479 was forced to turn away from the side chain of Tyr502 after **92A** was bound. Instead, the imidazole group of His479 formed one hydrogen bond with the backbone oxygen atom of Leu475 for 85.3% of the simulation time and formed one hydrogen bond with the amide linker of **92A** (-N···H–N- type, 71.8%). The *para*-chloride-substituted phenylethyl group of the inverse agonist **92A** also protruded into the steric gap between the side chains of His479 and Trp317 and formed π–π stacking interactions with them for 91.6% and 99% of the simulation, respectively.

Due to such intercalation of the inverse agonist **92A** into the triplet His479–Tyr502–Phe506 of the RORγt LBD structure, it could be reasonably expected that the local structures around H11, H11′, and H12 were seriously perturbed or distorted, and thus, H12 was destabilized. As shown in Fig. 9 for the structural information along the MD simulations, the helix H11 moved outwards approximately 5.1 Å (left panel of Fig. 9a), which would very possibly push away the H11′ and H12 from their original position. As a result of such a steric push, H11′ and H12 uncoiled after ~60 ns of the MD simulations (as shown in the right panel of Fig. 9a, and the blue curve in Fig. 2 shows the rmsd change at approximately 60 ns of the MD trajectory). Furthermore, a PCA plot (Fig. 9b) shows that the overall RORγt 5VB5 structure is much more flexible than the apo-form RORγt 5VB3 structure (Fig. 3a), particularly at the local regions of H2, H4, H11′, and H12. The destabilized and distorted H11′ and H12 would definitely make the RORγt LBD not able to recruit any cofactor molecule.

Inverse agonism for RORγt from the binding at the allosteric site
The structural dynamics of the apo-form RORγt 5VB3 system (Fig. 3a), the agonist-bound 5VB7 system (Fig. 7b), and the inverse agonist-bound 5VB5 system (Fig. 9b) show that the activation function loop H11′ is always flexible and possibly acts as a hinge between helices H11 and H12. It will be beneficial to design a small molecule to directly intercalate among the triplet His479–Tyr502–Phe506 residues and reorientate H12. This strategy to design novel inverse agonists will be more advantageous than the design of inverse agonists binding at the orthosteric-binding pocket, at least avoiding the possible competitive binding with natural ligands such as cholesterol [21]. Fortunately, and surprisingly, a recent study [17] identified an allosteric-binding site that was induced by the inverse agonist **4F1** and formed among the helices H4, H5, and H11, loop H11′ and helix H12. We performed MD simulations on the 5C4O system for the RORγt LBD bound to the inverse agonist **4F1** [17] to test the dynamics of the binding structure and stability of the reorientated H12.

As shown in Fig. 10, the inverse agonist **4F1** binding at this allosteric-binding site formed extensive interactions with residues Val480, Leu483, Gln484, Ala497, Phe498, and Leu505 and Phe506 from H12. In particular, the 2,6-disubstituted benzene ring of compound **4F1** formed a good π-π stacking interaction with the aromatic side chain of Phe506. The sulfonyl head of compound

MD simulations on RORγt: insights into its agonism and inverse agonism
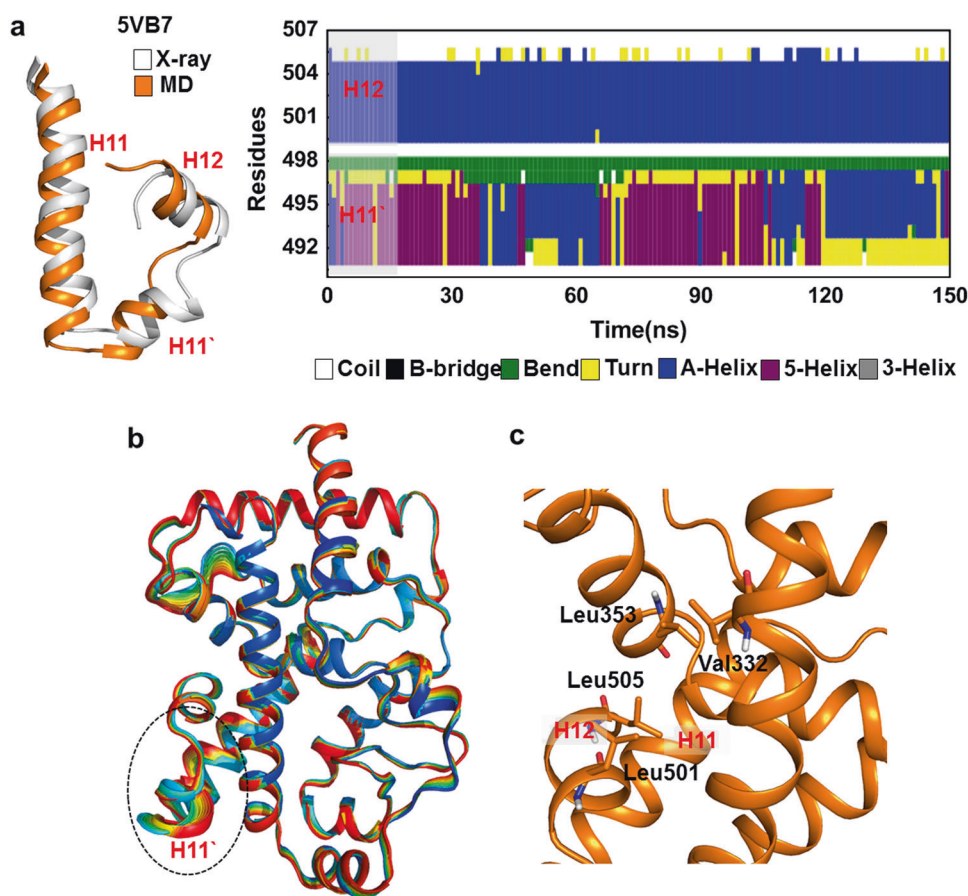CM Yuan et al.

1486

Fig. 7 The monitored structural information of the agonist-bound RORγt 5VB7 from MD trajectory. **a** The changes in the secondary structure of H11' and H12, which were tracked and calculated by using the DSSP software [37]. Left panel: one typical conformation of H11–H11'–H12 (in gold color) derived from the largest conformational cluster of the MD trajectory, is superimposed with that in the starting X-ray structure (in gray color). Right panel: secondary structure contents of H11' and H12 tracked along the MD simulations. **b** The PCA plot for the dynamics of the whole structure, and the H11' is labeled. **c** The representative hydrophobic cluster (V332, L353, and L501, L505 from H12, shown as sticks) at the protein-binding site of RORγt 5VB7 system, to be ready to match the typical hydrophobic motif LXXLL in a coactivator like SRC2 [20].
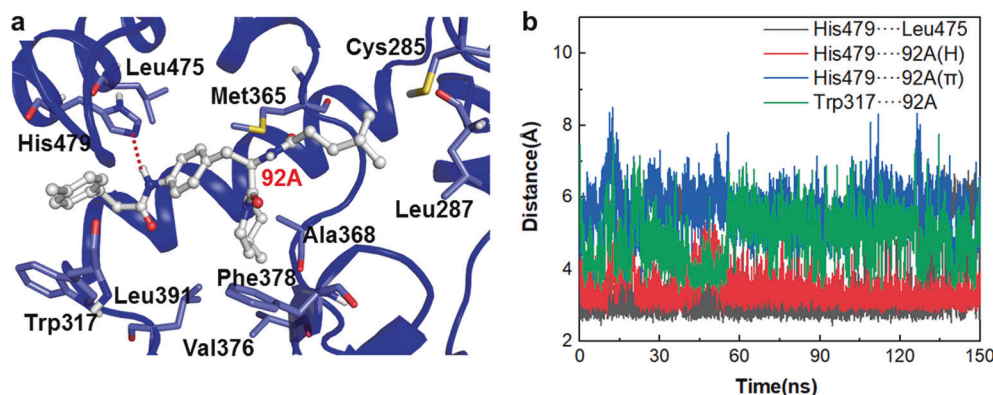

Fig. 8 The binding mode of an inverse agonist in the RORγt 5VB5 system. **a** The inverse agonist **92A** (shown in ball-and-stick style) at the orthosteric-binding pocket, the important residues interacting with **92A** are displayed in stick style. Hydrogen bonds are represented as red dashed lines. **b** The tracked distances between the important residues and the inverse agonist **92A**. The His479—Leu475 stands for the distance from the nitrogen atom at the His479 side chain to the backbone oxygen atom of Leu475, the His479—**92A**(H) stands for the tracked distance of the hydrogen-bonding interaction as shown in (**a**), and the His479—**92A**(π), Trp317—**92A** for their π–π stacking interactions, respectively

4F1 also formed hydrogen-bonding interactions with the backbone amide hydrogen atom of Ala497 (54% of the simulation time), amide hydrogen atom of Phe498 (26%), and side chain of Gln329 (1.5%).

Due to the binding of inverse agonist **4F1** at the allosteric-binding site, H12 is reorientated to a different position from that in the apo-form RORγt 5VB3 system (Fig. S1). We tracked the secondary structures of H11' and H12 and the molecular motion of
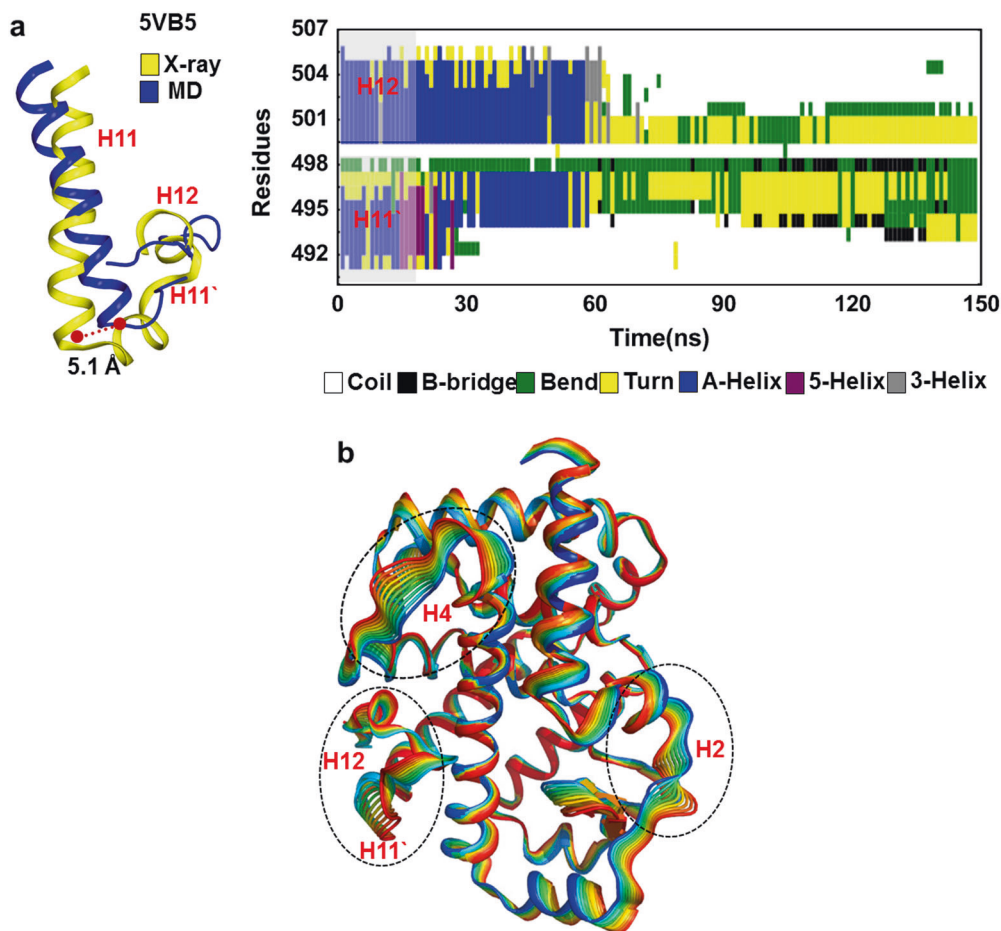
MD simulations on RORγt: insights into its agonism and inverse agonism
CM Yuan et al.

1487

Fig. 9 Structural dynamics of the inverse agonist **92A** binding at the orthosteric-binding pocket of RORγt 5VB5 system. **a** The tracked secondary structure of H11' and H12 in the RORγt 5VB5 system, which were calculated by using the DSSP software [37]. Left panel: one typical conformation of H11–H11'-H12 (colored in blue) derived from the largest conformational cluster based on the MD trajectory, is superimposed with that in the starting X-ray structure (in yellow color). Right panel: secondary structure contents of H11' and H12 tracked along the time of MD simulations. **b** The PCA plot for the dynamics of the receptor, also labeled the structural parts with obvious motion at H2, H4, H11', and H12
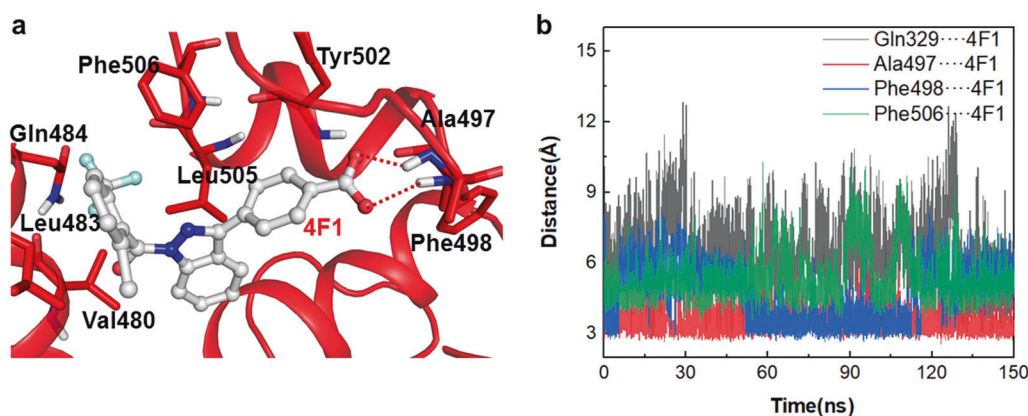

Fig. 10 The binding of the inverse agonist at the allosteric-binding site of the RORγt 5C4O system. **a** The inverse agonist **4F1** (shown in ball-and-stick style) at the binding site, the important residues interacting with **4F1** are displayed in stick style. Hydrogen bonds are represented as red dashed lines. **b** The tracked distances between the important residues and the inverse agonist **4F1**

the RORγt LBD in the 5C4O system. The results are shown in Fig. 11. As expected, H12 survived as a regular α-helix throughout the MD simulation, while H11' existed as a loop (Fig. 11a). A PCA plot (Fig. 11b) shows that the structure of H2 and the neighboring

β-sheet are obviously flexible, which are similar to what was observed in the apo-form RORγt 5VB3 system (Fig. 3a), mostly because the orthosteric-binding pocket is empty in the 5C4O system. Since H12 is reorientated and not able to form the
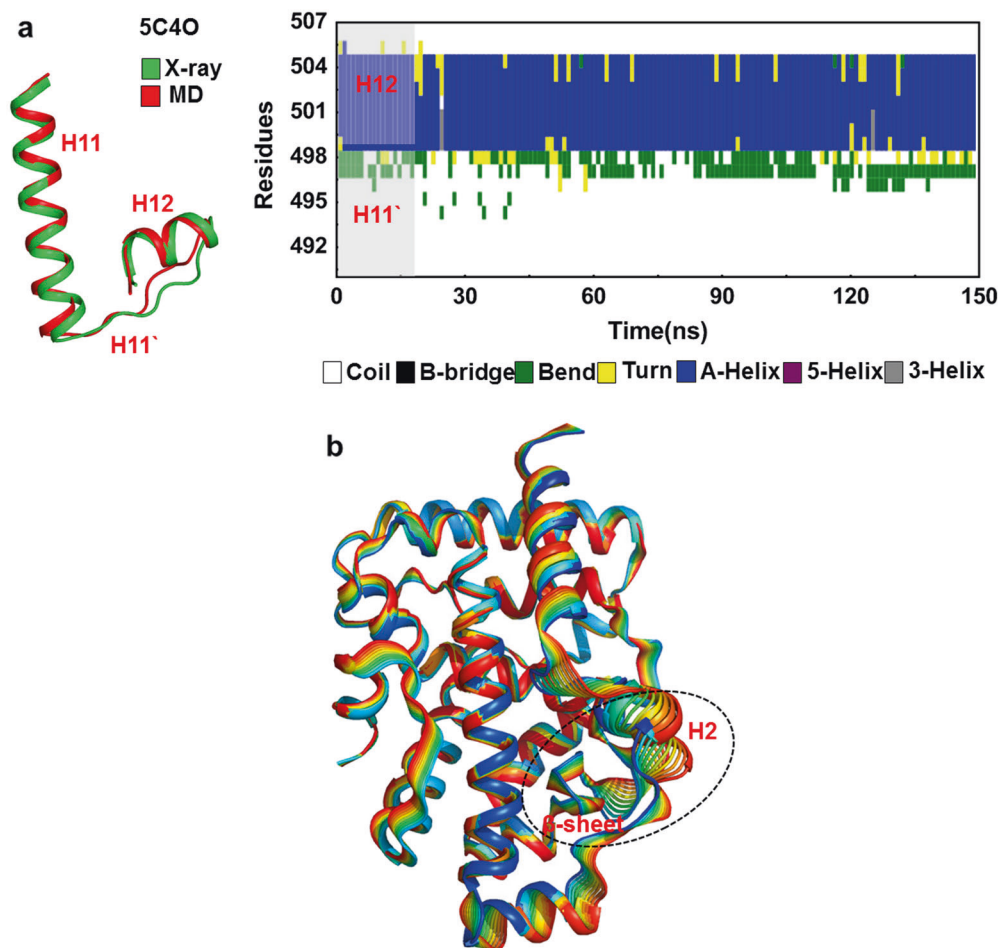
MD simulations on RORγt: insights into its agonism and inverse agonism
CM Yuan et al.

1488

Fig. 11 Tracked MD of the inverse agonist binding at the allosteric-binding site of RORγt 5C4O system. **a** The secondary structure of H11' and H12 in the RORγt 5C4O system, which was calculated by using the DSSP software [37]. Left panel: typical conformation of H11–H11'–H12 (colored in red) derived from the largest conformational cluster based on the MD trajectory, is superimposed with that in the starting X-ray structure (in green color). Right panel: secondary structure contents of H11' and H12 tracked along the time of MD simulations. **b** The PCA plot for the dynamics of the receptor, labeled at the structural parts with obvious motion at H2, and the β-sheet

protein-binding site, as observed in the apo-form RORγt 5VB3 system, it is definitely impossible for RORγt to recruit a coactivator, and therefore, its transcription function would be completely disrupted.

CONCLUSION

In summary, by performing MD simulations on the four different RORγt systems, we explored the molecular mechanisms of the agonism and inverse agonism of this receptor. We found that the orthosteric-binding pocket of the apo-form RORγt structure 5VB3 is mostly open and ready to accept an agonist, making the apo-form RORγt somewhat constitutively active. Once an agonist is bound at the orthosteric-binding pocket in the RORγt 5VB7 system, the helical structure of H12 is stabilized by strong triplet His479–Tyr502–Phe506 intramolecular interactions. The stabilized H12 helps RORγt to form the protein-binding site and therefore makes the receptor ready to recruit a coactivator molecule. The transcription function of RORγt can be interrupted by the binding of an inverse agonist at the orthosteric-binding pocket. The inverse agonist **92A**, which is bound at the orthosteric-binding pocket in the RORγt 5VB5 system, clashed sterically with the side chain of His479, destabilized the triplet His479–Tyr502–Phe506, and completely collapsed the structure of

H11' and H12. The transcription function of RORγt can also be interrupted by the inverse agonist **4F1** binding at the allosteric-binding site in the RORγt 5C4O system. The inverse agonist **4F1** directly intercalated into the triplet His479–Tyr502–Phe506, reorientated H12, and destroyed the presumed protein-binding site. The tracked intermolecular and intramolecular interactions from the MD simulations explicitly demonstrate the conformational dynamics and molecular mechanisms of how the RORγt receptor is activated by binding an agonist at the orthosteric-binding pocket and how the RORγt is inversely agonized by destabilizing H12 or reorienting H12 to a different position.

AUTHOR CONTRIBUTIONS

CMY and WF designed the work; HHC performed the docking studies; CMY and HHC performed the MD simulations; CMY, NNS, and XJM analyzed the trajectories from MD simulations; CMY, JX, and WF organized, discussed, and wrote the work.

MD simulations on RORγt: insights into its agonism and inverse agonism
CM Yuan et al.

1489

ADDITIONAL INFORMATION

REFERENCES

1. Burris T, Busby SA, Griffin PR. Targeting orphan nuclear receptors for treatment of metabolic diseases and autoimmunity. Chem Biol. 2012;19:51–59.
2. Lee JS, Cua DJ. The emerging landscape of RORγt biology. Immunity . 2014;40:451–2.
3. Isono F, Fujita-Sato S, Ito S. Inhibiting RORγt/Th17 axis for autoimmune disorders. Drug Discov Today. 2014;19:1205–11.
4. Rutz S, Eidenschenk C, Kiefer JR, Ouyang W. Post-translational regulation of RORγt-A therapeutic target for the modulation of interleukin-17-mediated responses in autoimmune disease. Cyto Grow Fact Rev. 2016;30:1–17.
5. Matsuyama M, Ishii Y, Sakurai H, Ano S, Morishima Y, Yoh K, et al. Overexpression of RORγt enhances pulmonary inflammation after infection with mycobacterium avium. PLoS ONE. 2016;11:e0147064. https://doi.org/10.1371/journal.pone.0147064.
6. Jetten AM, Takeda Y, Slominski A, Kang HS. Retinoic acid-related orphan receptor γ (RORγ): connecting sterol metabolism to regulation of the immune system and autoimmune disease. Curr Opin Toxicol. 2018;8:66–80.
7. Qiu R, Wang Y. Retinoic acid receptor-related orphan receptor γt (RORγt) agonists as potential small molecule therapeutics for cancer immunotherapy. J Med Chem. 2018;61:5794–804.
8. Cege C, Schluter T, Hoffmann T. Identification of the first inverse agonist of retinoid-related orphan receptor (ROR) with dual selectivity for RORb and RORγt. Bioorg Med Chem. 2014;24:5265–7.
9. Wang Y, Yang T, Liu Q, Ma Y, Yang L, Zhou L, et al. Discovery of N-(4-aryl-5-aryloxy-thiazol-2-yl)-amides as potent RORγt inverse agonists. Bioorg Med Chem. 2015;23:5293–302.
10. Wang Y, Cai W, Cheng Y, Yang T, Liu Q, Zhang G, et al. Discovery of biaryl amides as potent, orally bioavailable, and CNS penetrant RORγt inhibitors. ACS Med Chem Lett. 2015;6:787–92.
11. Abdel-Magid AF. RORc modulators for the treatment of autoimmune diseases. ACS Med Chem Lett. 2015;6:958–60.
12. Huang Y, Yu M, Sun N, Tang T, Yu F, Song X, et al. Discovery of carbozole carboxamides as novel RORγt inverse agonists. Eur J Med Chem. 2018;148:465–76.
13. Jin L, Martynowski D, Zheng S, Wada T, Xie W, Li Y. Structural basis for hydroxycholesterols as natural ligands of orphan nuclear receptor RORγ. Mol Endocrinol. 2010;24:923–9.
14. Yang T, Liu Q, Cheng Y, Cai W, Ma Y, Yang L, et al. Discovery of tertiary amine and indole derivatives as potent RORγt inverse agonists. ACS Med Chem Lett. 2014;5:65–68.
15. Fauber B, Magnuson S. Modulators of the nuclear receptor retinoic acid receptor-related orphan receptor-γ (RORγ or RORc). J Med Chem. 2014; 57:5871–92.
16. Xu HE. Family reunion of nuclear hormone receptors: structures, diseases, and drug discovery. Acta Pharmacol Sin. 2015;36:1–2.
17. Scheepstra M, Leysen S, van Almen GC, Miller JR, Piesvaux J, Kutilek V, et al. Identification of an allosteric binding site for RORγt inhibition. Nat Commun. 2015;6:8833.
18. Marcotte DJ, Liu Y, Little K, Jones JH, Powell NA, Wildes CP, et al. Structural determinant for inducing RORγ specific inverse agonism triggered by a synthetic benzoxazinone. BMC Struct Biol. 2016;16:1–9.
19. Olsson RI, Xue Y, von Berg S, Aagaard A, McPheat J, Hansson E, et al. Benzoxazepines achieve potent suppression of IL-17 release in human T-helper 17 (T$_H$17) cells through an induced-fit binding mode to the nuclear receptor RORγ. ChemMedChem. 2016;11:207–16.
20. Li X, Anderson M, Collin D, Muegge I, Wan J, Brennan D, et al. Structural studies unravel the active conformation of apo RORgt nuclear receptor and a common inverse agonism of two diverse classes of RORγt inhibitors. J Biol Chem. 2017;292:11618–30.
21. Kallen J, Izaac A, Be C, Arista L, Orain D, Kaupmann K, et al. Structural states of RORγt: X-ray elucidation of molecular mechanisms and binding interactions for natural and synthetic compounds. ChemMedChem. 2017; 12:1014–21.
22. Wang Y, Cai W, Tang T, Liu Q, Yang T, Yang L, et al. From RORγt agonists to two types of RORγt inverse agonists. ACS Med Chem Lett. 2018;9:120–4.
23. Narjes F, Xue Y, von Berg S, Malmberg J, Lliinas A, Olsson RI, et al. Potent and orally bioavailable inverse agonists for RORγt resulting from structure-based design. J Med Chem. 2018;61:7796–813.
24. Wu X, Wang R, Xing Y, Xue X, Zhang Y, Lu Y, et al. Discovery and structural optimization of 4-(4-(benzyloxy)phenyl)-3,4-dihydropyrimidin-2(1H)-ones as RORc inverse agonists. Acta Pharmacol Sin. 2016;37:1516–24.
25. Sastry GM, Adzhigirey M, Day T, Annabhimoju R, Sherman W. Protein and ligand preparation: parameters, protocols, and influence on virtual screening enrichments. J Comput Aid Mol Des. 2013;27:221–34.
26. Schuttelkopf AW, van Aalten DMF. PRODRG: a tool for high-throughput crystallography of protein-ligand complexes. Acta Cryst. 2004;D60:1355–63.
27. Abraham MJ, van der Spoel D, Lindahl E, Hess B, and the GROMACS development team. GROMACS User Manual version 5.1.4, Available from: www.gromacs.org, 2016.
28. Bian Y, He X, Jing Y, Wang L, Wang J, Xie X. Computational systems pharmacology analysis of cannabidiol: a combination of chemogenomics- knowledgebase network analysis and integrated in silico modeling and simulation. Acta Pharmacol Sin. 2019;40:374–86.
29. Nose S. A unified formulation of the constant temperature molecular dynamics methods. J Chem Phys. 1984;81:511–9.
30. Hoover WG, holian BL. Kinetic moments method for the canonical ensemble distribution. Phys Lett. 1996;211:253–7.
31. Parrinello M, Rahman A. Crystal structure and pair potentials: a molecular dynamics study. Phys Rev Lett. 1980;45:1196–9.
32. Parrinello M, Rahman A. Polymorphic transitions in single crystals: a new molecular dynamics method. J Appl Phys. 1981;52:7182–90.
33. Hess B, Bekker H, Berendsen HJC, Fraaije JGEM. LINCS: a linear constraint solver for molecular simulations. J Comput Chem. 1997;18:1463–72.
34. Ewald PP. Evaluation of optical and electrostatic lattice potentials. Ann Phys. 1921;369:253–87.
35. Essmann U, Perera L, Berkowitz ML, Darden T, Lee H, Pedersen LG. A smooth particle mesh Ewald method. J Chem Phys. 1998;103:8577–93.
36. Huang Z, Zhao J, Deng W, Chen Y, Shang J, Song K, et al. Identification of a cellular active SIRT6 allosteric activator. Nat Chem Biol. 2018;14:1118–26.
37. Wolfgang K, Christian S. Dictionary of protein secondary structure: pattern recognition of hydrogen-bonded and geometrical features. Biopolymers. 1983;22:2577–637.
38. Hotelling H. Analysis of a complex of statistical variables into principal components. J Educ Psychol. 1933;24:417–41.
39. Amadei A, Linssen AB, Berendsen HJ. Essential dynamics of proteins. Proteins. 1993;17:412–25.
40. David CC, Jacobs DJ. Principal component analysis: a method for determining the essential dynamics of proteins. Methods Mol Biol. 2014;1084:193–226.
41. Jiang H, Deng R, Yang X, Shang J, Lu S, Zhao Y, et al. Peptidomimetic inhibitors of APC-Asef interaction block colorectal cancer migration. Nat Chem Biol. 2017;13:994–1001.
42. Shen Q, Cheng F, Song H, Lu W, Zhao J, An X, et al. Proteome-scale investigation of protein allosteric regulation perturbed by somatic mutations in 7,000 cancer genomes. Am J Hum Genet. 2017;100:5–20.
43. The PyMOL Molecular Graphics System, Version 1.2r3pre, Schrödinger, LLC.